Laterality and interhemispheric integration in the larval *Drosophila* olfactory system

David M. Zimmerman[1,3,4], Benjamin L. de Bivort[2,4], and Aravinthan D. T. Samuel[3,4]

[1]Graduate Program in Biophysics, Harvard University
[2]Department of Organismic and Evolutionary Biology, Harvard University
[3]Department of Physics, Harvard University
[4]Center for Brain Science, Harvard University

March 2, 2025

Abstract

All animals with bilateral symmetry must integrate the sensory input from the left and right sides of their bodies to make coherent perceptual decisions. In *Drosophila* larvae, connectomic evidence suggests that olfactory signals from the two sides of the head are initially processed independently (as in the mammalian olfactory system) before being combined in the central brain. By pairing volumetric calcium imaging in intact larvae with microfluidic odor delivery and targeted laser ablation at the sensory periphery, we have mapped the propagation of olfactory signals between the two brain hemispheres, across successive layers of the larval olfactory system. This approach implicates the mushroom body (MB) as a key substrate for interhemispheric integration of odor representations. Whereas the two larval MBs appear to process odors largely independently at the level of their intrinsic neurons (Kenyon cells), the modulatory neurons of the MB show strongly symmetrized responses to asymmetric olfactory stimuli. Nevertheless, odor responses in some MB output neurons (MBONs), up to 5 synapses downstream from the sensory periphery, preserve information about stimulus laterality. Moreover, we show that asymmetric activation of these MBONs can modulate the animal's turning behavior in a side-biased manner. These findings

suggest that the deeply lateralized architecture of the larval olfactory system balances the need for interhemispheric integration with the advantages of parallel sensory processing.

1 Introduction

Any animal with bilateral symmetry must combine the two parallel streams of sensory input originating from the two sides of its body into a single unified representation of the world. Such interhemispheric integration (IHI) is a necessary prerequisite for transforming spatially and temporally disparate sensory signals into coherent motor commands. Neurological conditions in which IHI is compromised invariably lead to severely impaired perceptual decision making and disordered sensorimotor coordination (Gazzaniga et al. 1962). Even so, it is often advantageous for animals to process bilateral sensory signals in such a way that their spatial structure can be exploited. For instance, many animal species use interocular disparities to perceive depth (Qian 1997), interaural timing differences to localize sounds (Bernstein 2001), and internasal odor gradients to navigate in chemical landscapes (Rajan et al. 2006). The ability to selectively integrate or compare sensory information across hemispheres allows animals to sharpen their sensitivity to stimuli and adapt their behavioral responses to dynamic environments. However, it is poorly understood how bilaterian nervous systems implement these two different types of sensory processing in a balanced and mutually compatible way.

Recent work in rodent and primate models has begun to explore the circuit mechanisms underlying flexible IHI of somatosensory (Li et al. 2015; Li et al. 2016), auditory (Pacheco et al. 2021), and olfactory maps (Imai and Sakano 2008; Grimaud et al. 2024; Kuruppath et al. 2021). The case of mammalian olfaction has attracted particular interest due to the apparently ipsilateral nature of the afferents to cortex combined with the lack of topographic organization in piriform odor representations. These neuroanatomical features are difficult to reconcile with demonstrations of interhemispheric transfer of learned olfactory associations and reports that individual cortical neurons exhibit similar tuning to both ipsilateral and contralateral stimuli (Imai and Sakano 2008). Several alternative hypotheses have been suggested, including indirect excitatory coupling between

cognate glomeruli in the left and right olfactory bulbs and sculpting of interhemispheric connectivity at the cortical level by experience-dependent plasticity (Grimaud et al. 2024; Kuruppath et al. 2021). Unfortunately, the sheer size and complexity of the mammalian brain, the lack of a detailed wiring diagram for the mouse olfactory system, as well as the practical limitations of currently available neurogenetic tools, have hindered efforts to test these hypotheses in a precise and systematic way.

The olfactory system of the *Drosophila* larva is strikingly similar in its basic organization to that of most vertebrates. In *Drosophila* as in mammals, all ORNs expressing a given olfactory receptor (OR) type converge onto a corresponding glomerulus in the first olfactory neuropil, the antennal lobe (AL), which is the insect counterpart of the mammalian olfactory bulb. However, whereas ORNs in the antennae of the adult fly project bilaterally to both the left and right ALs (Gaudry et al. 2013), ORNs in the left and right dorsal organs (DOs) of the larva project almost exclusively to the ipsilateral AL (Fig. 1A), as in mammals. The larval olfactory system also has the remarkable property that each of the 21 ORN types is instantiated by a single left/right pair of cells. As a result, the input to any given glomerulus can be completely controlled by manipulating a single sensory neuron.

In the AL, a population of 21 uniglomerular projection neurons (uPNs) innervate the 21 olfactory glomeruli in a one-to-one manner and project ipsilaterally (with one exception) to two higher brain areas: the mushroom body (MB) and lateral horn (LH). (Only one pair of uPNs, corresponding to the Or35a input channel, receive input from both the ipsi- and contralateral DOs and send output to downstream areas in both the ipsi- and contralateral hemispheres.) A previous project led by our lab to map the complete wiring diagram of the first-instar (L1) larval AL also revealed the existence of 14 multiglomerular projection neurons (mPNs), which form synapses with multiple ORN types and project to a diverse set of higher brain areas (Berck et al. 2016). Notably, 4 mPNs per AL receive some degree of bilateral input, and 3 of these also produce bilateral output. In total, however, ORNs form 18x more synapses with ipsilateral PNs than with contralateral PNs (Berck et al. 2016). Thus, the larval AL circuitry is overwhelmingly unilateral in character.

In contrast, the wiring diagram of the larval MB suggests a much greater degree of interhemi-

spheric crosstalk (Fig. 1A). The L1 larval MB contains approximately 100 intrinsic neurons, called Kenyon cells (KCs), each of which receives input from a random subset of 1–6 PNs (Eichler et al. 2017). This population of KCs then converges onto a multilayered recurrent network of 24 MB output neurons (MBONs), which send output to many regions of the dorsal brain. The MBON dendrites arborize in spatially disjoint compartments collectively tiling the KC axons in such a way that every KC forms en passant synapses with most MBONs. Each compartment is also innervated by 1–3 MB input neurons (MBINs), capable of heterosynaptically modulating the strength of the corresponding KC-MBON connections in response to positive or negative reinforcement according to a compartment-specific learning rule (Hige et al. 2015).

Previous studies have implicated multilayered connectivity within the MBON network itself and indirect, convergent feedback from MBONs onto MBINs as possible mechanisms of multimodal sensory integration (Okray et al. 2023), memory consolidation,(Cervantes-Sandoval et al. 2017) and predictive learning (Eschbach et al. 2020). However, the functional significance of the complex interhemispheric connectivity in this circuit has received comparatively little attention. In this study, I show that olfactory processing preserves information about stimulus laterality even up to the output layer of the MB. Surprisingly, I find that odor responses in some MBONs—up to 5 synapses downstream from the sensory periphery—still exhibit side-specific or side-biased odor responses. In contrast, the MBIN "teaching signal" appears to be highly symmetrized, probably reflecting the dominant contribution of feedback from downstream brain areas. Finally, I dissect the contribution of several individual MBON types to odor-guided steering, revealing that asymmetric activation of specific MBONs can modulate the animal's turning behavior in a side-biased manner. These findings suggest that the deeply lateralized architecture of the larval olfactory system may have functional importance for the way that the larval fly processes olfactory signals in support of perceptual decision-making.

2 Methods

2.1 Fly husbandry and genetics

Flies were reared at 22 °C at 60% RH and a 12/12 LD cycle in vials containing standard cornmeal-based white food. To collect larvae for imaging and behavior experiments, adult flies were allowed to lay eggs on grape juice agar plates supplemented with fresh yeast paste, following standard protocols (Featherstone et al. 2009). Calcium imaging experiments were performed in late L1 larvae (2 days after egg laying [AEL]), while behavioral experiments were performed in early L3 larvae (3–4 days AEL). Throughout this paper, the following driver lines were used to target genetically defined subsets of neurons:

cell type	driver line
KCs	*R14H06-GAL4*
MBINs	*Vmat-T2A-GAL4*
MBON-a1	*SS02006 split-GAL4*
MBON-c1	*SS01776 split-GAL4*
MBON-h1/h2	*SS00894 split-GAL4*
MBON-i1	*SS01726 split-GAL4*
MBON-m1	*SS02163 split-GAL4*
ORN 42a	*Or42a-GAL4* (III)
ORN 42b	*Or42b-GAL4* (II)

For imaging experiments, the following effector lines were used: *UAS-GCaMP6m*; *Orco-RFP* (Fig. 1) and *UAS-syt::GCaMP6s, MB247-RFP*; *Orco-RFP* (elsewhere).

For behavioral experiments involving stochastic optogenetic activation of individual MBONs (4), we used a stochastic labeling approach to produce animals expressing an mVenus-tagged CsChrimson transgene in a subset of cells labelled by a given MBON split-GAL4 line:

$$\frac{hsFLPD5}{(w)}; \frac{MBON\ split\text{-}GAL4}{UAS\text{-}FRT\text{-}stop\text{-}FRT\text{-}CsChrimson::mVenus;\ +}$$

Animals of this genotype were behaviorally profiled (see below) and subsequently examined under an inverted confocal microscope to identify the number of MBONs labelled (0, 1, or 2). For all stochastic labeling experiments, animals were raised at 25 °C to induce expression of FLP recombinase (in lieu of an acute heat shock).

2.2 Functional imaging and microfluidics

We used a previously described microfluidic platform for simultaneous odor delivery and calcium imaging of intact L1 larvae (Si et al. 2021). All experiments used an 8-channel microfluidic device. Stimuli consisted of 5 s odor pulses interleaved with 30 s water washout periods. Larvae of appropriate size were picked directly from grape plates, washed 3X with distilled water, and loaded into the microfluidic device using a 1 mL syringe filled with Triton X-100 (0.1%) solution. Each animal was positioned at the end of a narrow channel with its dorsal side facing the microscope objective. Fluorescent signal was recorded using an EMCCD camera (Andor iXon) attached to an inverted spinning-disk confocal microscope (Nikon). A 40X water immersion objective (Nikon; NA 1.15) was used for all live imaging experiments. A piezo scanner (PIFOC) was used to acquire 3D volumes, consisting of 18 ± 4 z-planes with a spacing of 1.5 µm, at a volumetric rate of approximately (0.9 ± 0.2) Hz.

2.3 Laser ablation

A pulsed dye laser (Andor Micropoint) integrated into the light path of our microscope was used to ablate the antennal nerve near its exit from the dorsal organ ganglion (DOG). The ORNs were genetically labeled via *Orco-RFP* for ease of targeting. Calcium imaging experiments were performed immediately after ablation to minimize the possibility of homeostatic compensatory changes following this perturbation.

2.4 Behavior and optogenetics

Single-animal optogenetic assays were performed by placing larvae in individual agarose-coated arenas of a 24-arena assay plate. This plate was then inserted into a behavior rig equipped with an overhead projector and IR camera, under the control of a custom MATLAB script. Light from the projector was passed through a 600 nm filter (Edmund Optics) to minimize visual stimulation. Larval trajectories were tracked via the MARGO software package (Werkhoven et al. 2019) and analyzed with MAGATAnalyzer (Gershow et al. 2012). For these experiments, larvae were reared on yeast paste supplemented with all-trans retinal (100 mM). The illumination intensity was $5\,\mu\mathrm{W\,mm^{-2}}$.

2.5 Image analysis

To extract calcium traces from volumetric recordings, data were first motion-corrected by group-wise nonlinear registration using the `itk-elastix` software package (Shamonin et al. 2013). The time-averaged 4D (3D + color channel) volumes were then manually annotated in `napari` to define ROIs for the desired cells and/or MB compartments (Chiu et al. 2022). Finally, time series corresponding to the 90th percentile of the raw fluorescence signal in each ROI were baseline-corrected for photobleaching and used to compute $\Delta F/F_0$ traces. The baseline fluorescence (F_0) was estimated from a time-average over the 5 s period immediately preceding stimulus onset, and the peak fluorescence was obtained as the maximum value of F during the stimulus period.

3 Results and Discussion

Although analysis of the L1 larval connectome suggests that feedforward connections into the KC layer are predominantly ipsilateral in character, KCs nevertheless receive a degree of contralateral axo-dendritic input from the mPN pathway as well as abundant, putatively excitatory axo-axonic feedback from contralateral MBINs (Fig. 1A). Therefore we first sought to characterize the extent of functional IHI in the layers of the olfactory system upstream of the MB. To this end, we used a microfluidic platform for simultaneous odor delivery and calcium imaging previously developed in

our lab (Si et al. 2019). This technique enables precise control over the timing and concentration but not spatial pattern of olfactory stimulation. In order to synthesize unilateral patterns of ORN activity, we used a pulsed UV laser to ablate the antennal nerve containing the ORN axon fibers, thus restricting sensory input to the intact side of the animal's head (Fig. 1B). We then recorded calcium responses in the KCs of the larval MB immediately after laser ablation.

Consistently across multiple monomolecular odorants, we observed strong odor-evoked responses in the KCs ipsilateral to the intact DOG (Fig. 1C, E–F) but virtually none on the contralateral side (Fig. 1D, E–F). Even the odorant 1-pentanol, which is notable for recruiting the unique input channel associated with the bilateral uPN 35a (Berck et al. 2016; Si et al. 2019), elicited only weak and sporadic contralateral KC responses. These data indicate that the numerically weak axo-dendritic input from contralateral mPNs and the strong axo-axonic feedback from contralateral MBINs does not produce a significant degree of functional coupling between the left and right hemipopulations of KCs. Thus, the two MBs appear to function largely independently from one another, implying that the primary loci of IHI must lie downstream of the KC layer.

In view of the strong, bilateral, and reciprocal connectivity between KCs and MBINs, we wondered if the MBIN ensemble would share the strikingly ipsilateral character of the KCs' responses to odors. To test this hypothesis, we imaged volumetrically from the MBIN presynaptic terminals in the MB lobes. By expressing presynaptically trafficked GCaMP6s in all MBINs under control of Vmat-T2A-GAL4 (along with *MB247-RFP* as an anatomical reference) and taking advantage of the anatomical stereotypy of the MB circuit, we were able to extract the MBIN activity in 9 of the 11 larval MB compartments. We observed strong and highly stereotyped odor-evoked responses in most MBIN compartments. However, in striking contrast to the KCs, each DAN compartment responded with a high degree of left–right symmetry to one-sided olfactory stimulation (Fig. 2A–D). After controlling for multiple comparisons, the difference in ipsi- vs. contralateral peak response amplitudes failed to reach statistical significance for any MBIN compartment (Fig. 2C). These functional data suggest that the MBIN ensemble may enforce IHI of learned odor associations by effectively symmetrizing the representation of reinforcements between the two brain hemispheres.

We next turned to the MBON ensemble, where connectomic evidence suggests a highly hetero-

geneous pattern of left–right crosstalk. In particular, some MBON types exhibit an almost perfectly ipsilateral (MBON-c1) or contralateral (MBON-m1) pattern of anatomical projections, while others (MBON-i1, -a1, -h1/h2) show more mixed ipsi/contralateral innervation at the level of their dendritic and/or axonal arbors (Fig. 3A–B) (Eichler et al. 2017; Saumweber et al. 2018; Winding et al. 2023). Using a collection of previously published split-GAL4 lines (Eschbach et al. 2021), we recorded presynaptic calcium responses to unilateral odor stimulation in 5 different MBON subtypes, chosen to provide a representative sample of the different innervation patterns. In agreement with the connectomic data, we observed that certain MBON output channels (notably MBON-c1 and -m1) almost perfectly preserve information about the laterality of a one-sided odor stimulus, with minimal mixing of the signal from the two DOGs (Fig. 3C–F). Similarly, MBON-a1 conveys a statistically significant ipsilateral bias in its presynaptic responses, despite sending a similar number of axon terminals to both brain hemispheres.

The most striking example of side-specificity was perhaps MBON-m1, which (despite its predominantly contralateral projection pattern) receives significant axo-dendritic input from the bilateral MBON-h1/h2. Indeed, the degree of multi-compartment input to MBON-m1—as well as the fact that it receives input not only from the MB but also from the LH—has led to its being called a "convergence neuron" and regarded as a key node in relaying the integrated output of the MB pathway to downstream premotor areas (Eschbach et al. 2020; Eschbach et al. 2021). In view of MBON-m1's evident importance in integrating the output of multiple arms of the olfactory system, it is somewhat counterintuitive that its responses would preserve the laterality of odor stimuli to such a high degree. However, this can be partly explained by the observation that MBON-h1/h2 and MBON-k1, which integrate bilateral KC input and make respectively 1- and 2-hop connections onto MBON-m1, likely release the inhibitory neurotransmitters GABA and glutamate (Eichler et al. 2017; Eschbach et al. 2021). Thus, the *excitatory* inputs onto MBON-m1 indeed appear to be predominantly unilateral in character.

This observation of side-specific odor tuning in the MBON layer suggested the possibility that asymmetric patterns of MBON activity might contribute to navigational control by biasing odor-guided steering. Consistent with this idea, connectomic analysis indicates that different MBONs

synapse to varying degrees onto postsynaptic neurons with hemispherically "unbalanced" axon arbors. MBON-m1 is particularly notable for having many postsynaptic partners with near exclusively ipsilateral or contralateral axon arbors (Fig. 4A). A similar conjecture has recently been made in the context of the adult fly brain, motivated by the observation that some adult MBONs (e.g., the "atypical" MBON32) synapse directly onto asymmetrically projecting descending neurons (e.g., DNa02) in a manner that might enable "see-saw" steering control (Rayshubskiy et al. 2024).

To test this possibility directly, we measured the effect of unilateral optogenetic activation of individual MBON types on the rate of ipsilateral and contralateral turning. Although no turn rate asymmetry was observed in the case of the avoidance-promoting MBON-h1/h2, a significantly greater stimulus-triggered change in the ipsiversive (vs. contraversive) turn rate was observed for both MBON-m1 and -a1 (Fig. 4C). The sign of this change was positive for the avoidance-promoting MBON-a1 and negative for the attraction-promoting MBON-m1. No such asymmetry was observed in control animals expressing the optogenetic effector in both hemispheres (Fig. 4B) or neither hemisphere (Fig. 4D).

In summary, we have shown that the left and right larval MBs exhibit a surprising degree of functional independence. Despite the existence of midline-crossing afferent input from contralateral mPNs and extensive bilateral feedback from MBINs, the KC populations in the two brain hemispheres show almost exclusively ipsilateral odor responses, indicating limited functional coupling between the left and right MBs. In contrast, the MBON ensemble, characterized by heterogeneous left-right anatomical connectivity, exhibits diverse degrees of side-specific odor tuning, with some subtypes like MBON-m1 faithfully transmitting the laterality of an odor stimulus. This asymmetry in hemispheric bias is not inherited from MBINs, whose uniformly symmetrized responses may be important for providing a coherent teaching signal to instruct experience-dependent changes in MBON firing. Optogenetic activation experiments further revealed that specific MBON types modulate turning in a side-biased manner, thus hinting at their potential role in navigational control of steering.

In all, these results argue that the architecture of the larval olfactory system balances the competing requirements for IHI and lateralized sensory processing by employing parallel output

channels with variously symmetrizing or anti-symmetrizing wiring motifs. This study lays the groundwork for future efforts to unravel how these diverse output channels differentially contribute to behavioral control of navigation and steering in naturalistic contexts.

References

Berck ME, Khandelwal A, Claus L, Hernandez-Nunez L, Si G, Tabone CJ, Li F, Truman JW, Fetter RD, Louis M, et al. 2016. The wiring diagram of a glomerular olfactory system. Elife 5:e14859. DOI: 10.7554/eLife.14859.

Bernstein LR. 2001. Auditory processing of interaural timing information: new insights. J Neurosci Res 66(6):1035–1046. DOI: 10.1002/jnr.10103.

Cervantes-Sandoval I, Phan A, Chakraborty M, Davis RL. 2017. Reciprocal synapses between mushroom body and dopamine neurons form a positive feedback loop required for learning. Elife 6:e23789. DOI: 10.7554/eLife.23789.

Chiu C.-L, Clack N, the napari community. 2022. napari: a Python Multi-Dimensional Image Viewer Platform for the Research Community. Microsc Microanal 28 (S1):1576–1577. DOI: 10.1017/S1431927622006328.

Eichler K, Li F, Litwin-Kumar A, Park Y, Andrade I, Schneider-Mizell CM, Saumweber T, Huser A, Eschbach C, Gerber B, et al. 2017. The complete connectome of a learning and memory centre in an insect brain. Nature 548(7666):175–182. DOI: 10.1038/nature23455.

Eschbach C, Fushiki A, Winding M, Afonso B, Andrade IV, Cocanougher BT, Eichler K, Gepner R, Si G, Valdes-Aleman J, et al. 2021. Circuits for integrating learned and innate valences in the insect brain. Elife 10:e62567. DOI: 10.7554/eLife.62567.

Eschbach C, Fushiki A, Winding M, Schneider-Mizell CM, Shao M, Arruda R, Eichler K, Valdes-Aleman J, Ohyama T, Thum AS, et al. 2020. Recurrent architecture for adaptive regulation of learning in the insect brain. Nat Neurosci 23(4):544–555. DOI: 10.1038/s41593-020-0607-9.

Featherstone DE, Chen K, Broadie K. 2009. Harvesting and preparing Drosophila embryos for electrophysiological recording and other procedures. J Vis Exp (27):1347. DOI: 10.3791/1347.

Gaudry Q, Hong EJ, Kain J, de Bivort BL, Wilson RI. 2013. Asymmetric neurotransmitter release enables rapid odour lateralization in *Drosophila*. Nature 493(7432):424–428. DOI: 10.1038/nature11747.

Gazzaniga MS, Bogen JE, Sperry RW. 1962. Some functional effects of sectioning the cerebral commissures in man. Proc Natl Acad Sci U S A 48:1765–1769. DOI: 10.1073/pnas.48.10.1765.

Gershow M, Berck M, Mathew D, Luo L, Kane EA, Carlson JR, Samuel AD. 2012. Controlling airborne cues to study small animal navigation. Nat Methods 9(3):290–296. DOI: 10.1038/nmeth.1853.

Grimaud J, Dorrell W, Jayakumar S, Pehlevan C, Murthy V. 2024. Bilateral Alignment of Receptive Fields in the Olfactory Cortex. eNeuro 11(11):ENEURO.0155–24.2024. DOI: 10.1523/ENEURO.0155-24.2024.

Hige T, Aso Y, Modi MN, Rubin GM, Turner GC. 2015. Heterosynaptic Plasticity Underlies Aversive Olfactory Learning in Drosophila. Neuron 88(5):985–998. DOI: 10.1016/j.neuron.2015.11.003.

Imai T and Sakano H. 2008. Interhemispheric olfactory circuit and the memory beyond. Neuron 58(4):465–467. DOI: 10.1016/j.neuron.2008.05.004.

Kuruppath P, Bai L, Belluscio L. 2021. Functional relevance of dual olfactory bulbs in olfactory coding. eNeuro 8(5):ENEURO.0070–21.2021. DOI: 10.1523/ENEURO.0070-21.2021.

Li N, Chen T.-W, Guo ZV, Gerfen CR, Svoboda K. 2015. A motor cortex circuit for motor planning and movement. Nature 519(7541):51–56. DOI: 10.1038/nature14178.

Li N, Daie K, Svoboda K, Druckmann S. 2016. Robust neuronal dynamics in premotor cortex during motor planning. Nature 532(7600):459–464. DOI: 10.1038/nature17643.

Okray Z, Jacob PF, Stern C, Desmond K, Otto N, Talbot CB, Vargas-Gutierrez P, Waddell S. 2023. Multisensory learning binds neurons into a cross-modal memory engram. Nature 617(7962):777–784. DOI: 10.1038/s41586-023-06013-8.

Pacheco DA, Thiberge SY, Pnevmatikakis E, Murthy M. 2021. Auditory activity is diverse and widespread throughout the central brain of Drosophila. Nat Neurosci 24(1):93–104. DOI: 10.1038/s41593-020-00743-y.

Qian N. 1997. Binocular disparity and the perception of depth. Neuron 18(3):359–368. DOI: 10.1016/s0896-6273(00)81238-6.

Rajan R, Clement JP, Bhalla US. 2006. Rats smell in stereo. Science 311(5761):666–670. DOI: 10.1126/science.1122096.

Rayshubskiy A, Holtz SL, Bates A, Vanderbeck QX, Capdevila LS, Wilson RI. 2024. Neural circuit mechanisms for steering control in walking Drosophila. eLife 13. Publisher: eLife Sciences Publications Limited. DOI: 10.7554/eLife.102230.1.

Saumweber T, Rohwedder A, Schleyer M, Eichler K, Chen Y.-C, Aso Y, Cardona A, Eschbach C, Kobler O, Voigt A, et al. 2018. Functional architecture of reward learning in mushroom body extrinsic neurons of larval Drosophila. Nat Commun 9(1):1104. DOI: 10.1038/s41467-018-03130-1.

Shamonin DP, Bron EE, Lelieveldt BPF, Smits M, Klein S, Staring M, Alzheimer's Disease Neuroimaging Initiative. 2013. Fast parallel image registration on CPU and GPU for diagnostic classification of Alzheimer's disease. Front Neuroinform 7:50. DOI: 10.3389/fninf.2013.00050.

Si G, Baron J, Feng Y, Samuel ADT. 2021. An olfactory pattern generator for on-demand combinatorial control of receptor activities. bioRxiv. DOI: 10.1101/2021.05.31.446433.

Si G, Kanwal JK, Hu Y, Tabone CJ, Baron J, Berck M, Vignoud G, Samuel ADT. 2019. Structured Odorant Response Patterns across a Complete Olfactory Receptor Neuron Population. Neuron 101(5):950–962.e7. DOI: 10.1016/j.neuron.2018.12.030.

Werkhoven Z, Rohrsen C, Qin C, Brembs B, de Bivort B. 2019. MARGO (Massively Automated Real-time GUI for Object-tracking), a platform for high-throughput ethology. PLoS One 14(11):e0224243. DOI: 10.1371/journal.pone.0224243.

Winding M, Pedigo BD, Barnes CL, Patsolic HG, Park Y, Kazimiers T, Fushiki A, Andrade IV, Khandelwal A, Valdes-Aleman J, et al. 2023. The connectome of an insect brain. Science 379(6636):eadd9330. DOI: 10.1126/science.add9330.

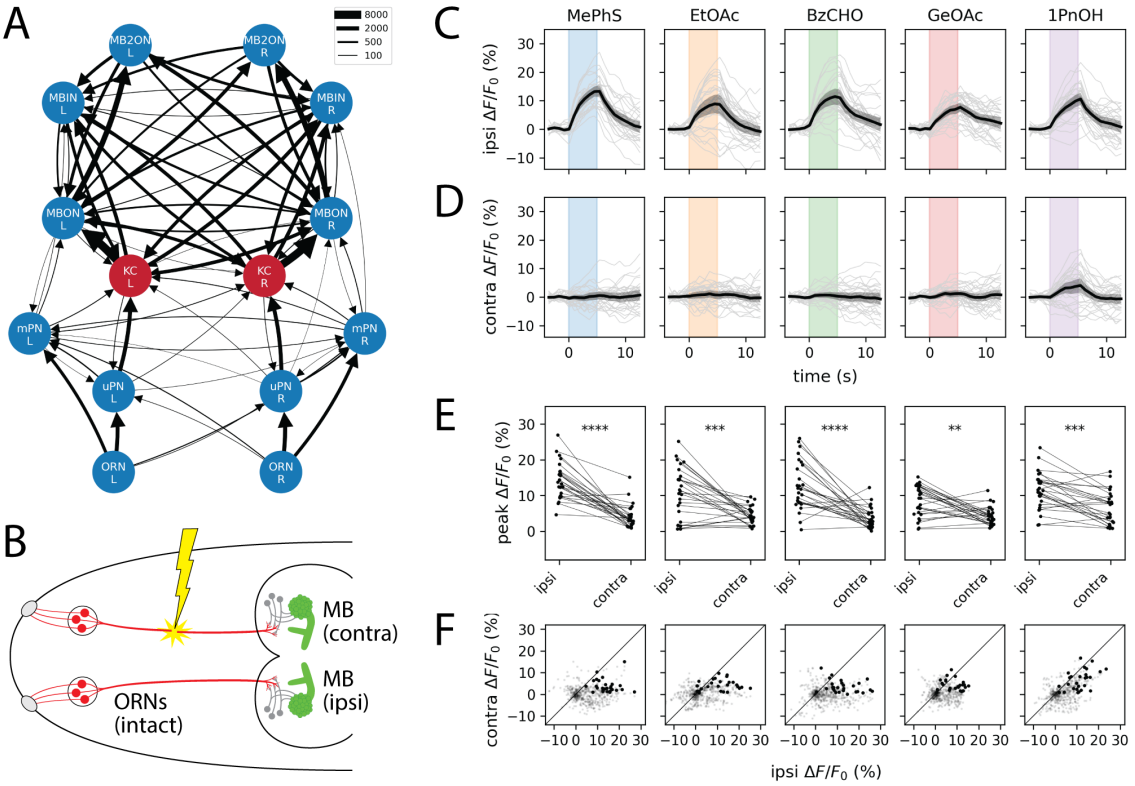

Figure 1: The mushroom body is the first major locus of olfactory IHI in the larval olfactory system. A. Summarized wiring diagram of the L1 larval olfactory system (Berck et al. 2016; Winding et al. 2023). Each node agglomerates all cells of the same class (ORNs, uPNs, mPNs, KCs, MBINs, MBONs, MB2ONs) in a given hemisphere. Edge width is proportional to the square root of the number of synapses between all cells in a given pair of cell types. B. Experimental scheme for synthesizing lateralized odor stimuli by laser ablation of the antennal nerve (red). The KCs of the larval MB are shown in green to represent transgenic expression of GCaMP for calcium imaging. C–F. KCs exhibit consistent ipsilateral and negligible contralateral odor responses. Plots depict ipsilateral (C) and contralateral (D) odor-evoked cytosolic GCaMP6m transients and peak ipsilateral vs. contralateral response amplitudes (E). In C and D, dark lines represent grand averages over $n = 9$ animals and 3 stimulus repetitions per animal; gray shaded regions are bootstrapped 95% CIs. Colored vertical bars represent 5 s stimulus periods. F. Scatter plots of ipsilateral and contralateral KC activity in the 15 s following stimulus onset. Bold points represent peak responses. Diagonal lines represent equality between ipsilateral and contralateral response amplitudes. Each column shows responses to a different odor. All odors were used at 10^{-4} (v/v) dilution. Odor abbreviations: MePhS, methyl phenyl sulfide (blue); EtOAc, ethyl acetate (orange); BzCHO, benzaldehyde (green); GeOAc, geranyl acetate (red); 1PnOH, 1-pentanol (violet). Statistics: **, $p_{\mathrm{adj}} < 0.01$; ***, $p_{\mathrm{adj}} < 0.001$; ****, $p_{\mathrm{adj}} < 0.0001$ (paired Student's t-test with Bonferroni correction).

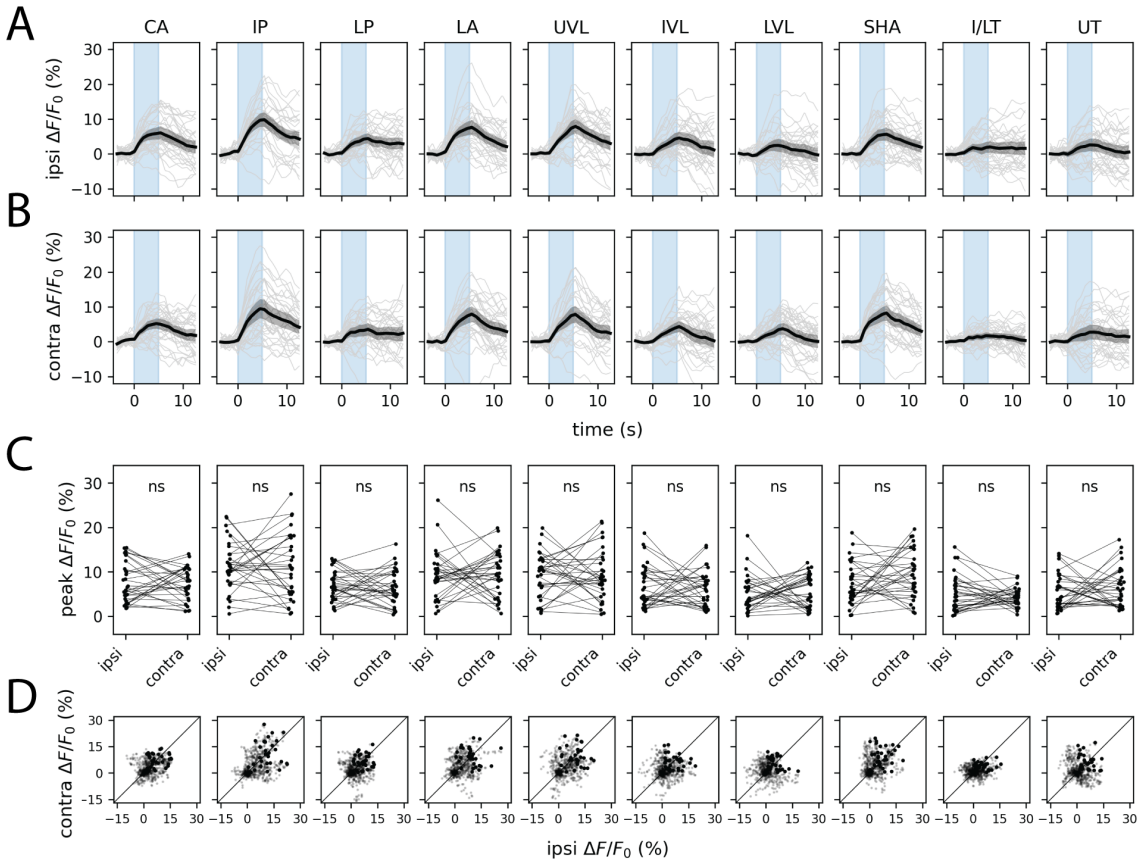

Figure 2: MBINs symmetrize asymmetric odor stimuli. Plots show ipsilateral (A) and contralateral (B) presynaptic GCaMP6s transients and peak ipsilateral vs. contralateral response amplitudes (C) evoked by one-sided stimulation with methyl phenyl sulfide (10^{-4}). In A and B, dark lines represent grand averages over $n = 8$ animals and 4 stimulus repetitions per animal; gray shaded regions are bootstrapped 95% CIs. Colored vertical bars represent 5 s stimulus periods. D. Scatter plots of ipsilateral and contralateral MBIN activity in the 15 s following stimulus onset. Bold points represent peak responses. Diagonal lines represent equality between ipsilateral and contralateral response amplitudes. Each column shows responses in a different anatomically defined MBIN compartment. One pair of MB compartments, the intermediate toe (IT) and lower toe (LT) of the medial lobe, could not be reliably distinguished and are thus combined for purposes of data visualization. Anatomical abbreviations: CA, calyx; IP, intermediate penduncle; LP, lower peduncle; LA, lateral appendix; UVL, upper vertical lobe; IVL, intermediate vertical lobe; LVL, lower vertical lobe; SHA, shaft; I/LT, intermediate/lower toe; UT, upper toe. Statistics: n.s., $p_{\text{adj}} \geq 0.05$ (paired Student's t-test with Bonferroni correction).

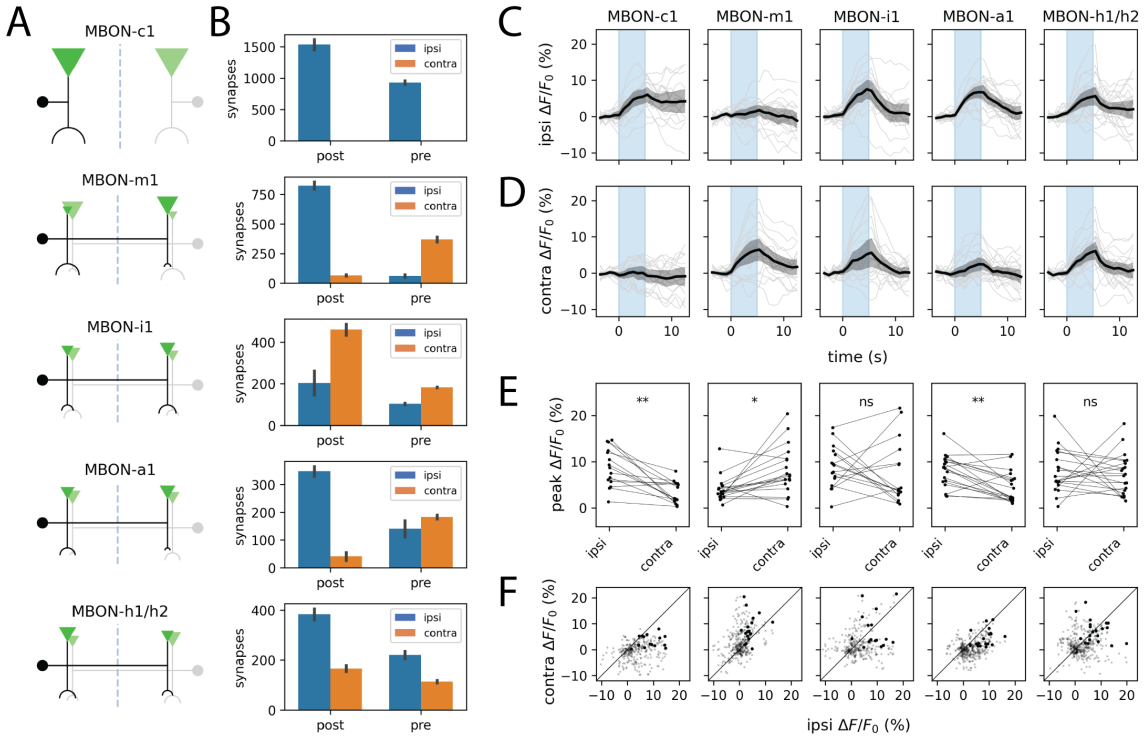

Figure 3: Different MBONs exhibit varying degrees of IHI. A. Schematic projection patterns of 5 different MBON types. Filled circles denote cell bodies. Inverted triangles and semicircular arcs denote pre- and postsynaptic sites, respectively; their size is proportional to the number of such sites per cell type. B. Quantification of ipsi-/contralateral distribution of pre-/postsynaptic sites for each of the MBON types shown in A. Error bars represent s.e.m. (which, for the case of $n = 2$ cells, is simply half of the absolute difference in counts). C–F. MBONs exhibit diverse ipsi- vs contralateral tuning to asymmetric odor stimuli. Plots show ipsilateral (C) and contralateral (D) presynaptic GCaMP6s transients and peak ipsilateral vs. contralateral response amplitudes (E) evoked by one-sided stimulation with methyl phenyl sulfide (10^{-4}). In C and D, dark lines represent grand averages over $n = 7 \pm 1$ animals and 3 stimulus repetitions per animal; gray shaded regions are bootstrapped 95% CIs. Colored vertical bars represent 5 s stimulus periods. D. Scatter plots of ipsilateral and contralateral MBIN activity in the 15 s following stimulus onset. Bold points represent peak responses. Diagonal lines represent equality between ipsilateral and contralateral response amplitudes. Each column shows responses in a specific MBON type, labeled by the corresponding split-GAL4 line (see Methods). Statistics: n.s., $p_{\mathrm{adj}} \geq 0.05$; *, $p_{\mathrm{adj}} < 0.05$; **, $p_{\mathrm{adj}} < 0.01$ (paired Student's t-test with Bonferroni correction).

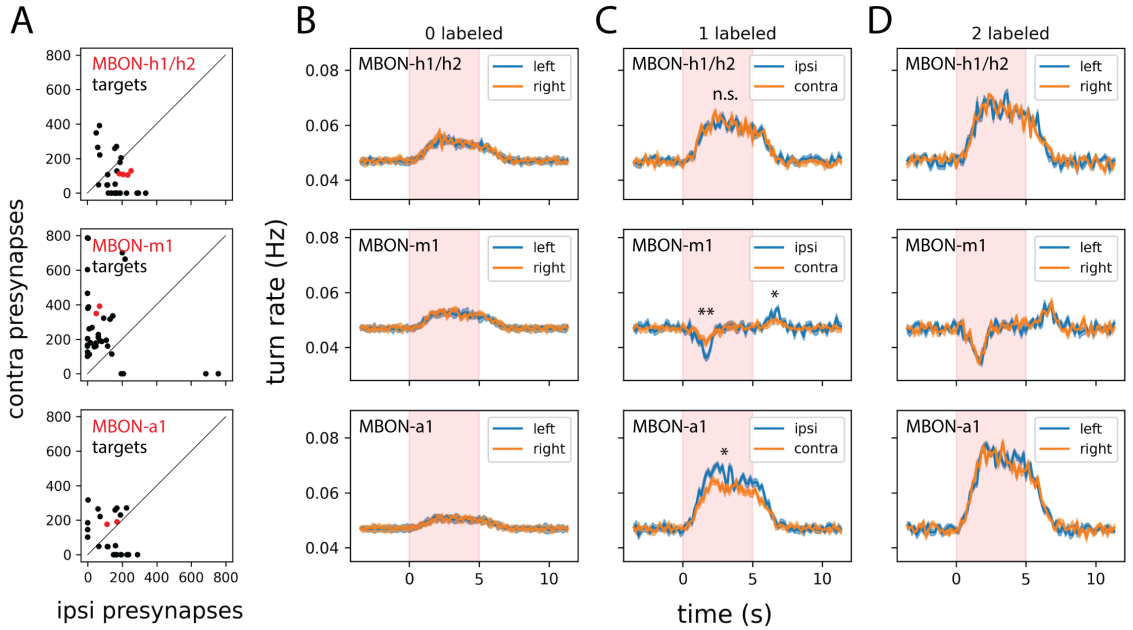

Figure 4: Different MBONs target variously lateralized downstream cell types and exert diverse effects on turning. A. Quantification of the number of ipsi-/contralateral presynaptic sites for all postsynaptic partners of the indicated MBON type. Data for the MBON itself are in red. B–D. Optogenetic activation of individual MBONs modulates turning in a variably side-biased manner. Plots depict the change in side-specific turn rates triggered by optogenetic stimulation of 0 (B), 1 (C), or 2 (D) cells of the indicated MBON type in each row. For the 2-cell case of MBON-h1/h2, animals expressed the optogenetic effector CsChrimson::mVenus in 1 cell of each hemisphere. Dark lines represent ensemble averages and shaded regions represent ±1 s.e.m. Statistics: n.s., $p_{\mathrm{adj}} \geq 0.05$; *, $p_{\mathrm{adj}} < 0.05$; **, $p_{\mathrm{adj}} < 0.01$ (unpaired Student's t-test with Bonferroni correction).